UNIVERSITAT POLITÈCNICA DE VALÈNCIA

Escola Tècnica Superior d'Enginyeria Agronòmica i del Medi Natural

# UNIVERSITAT POLITÈCNICA DE VALÈNCIA

## School of Agricultural Engineering and Environment

# Structural characterization of FmtA: a new esterase from Staphylococcus aureus.

End of Degree Project

Bachelor's Degree in Biotechnology

AUTHOR: Company Barber, Rebeca

Tutor: Porcel Roldán, Rosa Caridad

External cotutor: RAMON MAIQUES, SANTIAGO

ACADEMIC YEAR: 2023/2024

UNIVERSITAT POLITÈCNICA DE VALÈNCIA

Escola Tècnica Superior d'Enginyeria Agronòmica
i del Medi Rural (ETSEAMN)

School of Agricultural Engineering and Environment

# Structural characterization of FmtA: a new esterase from Staphylococcus aureus.

End of Degree Project

Bachelor's Degree in Biotechnology




Author: Company Barber, Rebeca

Tutor: Porcel Roldán, Rosa Caridad

External cotutor: Ramon Maiques, Santiago

Academic year: 2023-2024

Valencia, April 2024

**TITLE:** Structural characterization of FmtA: a new esterase from Staphylococcus aureus.

**SUMMARY**: FmtA is a penicillin-recognising protein with an esterase function that involves hydrolysing the ester bond linking D-alanine to the backbone of teichoic acids. It is a protein of interest because it acts on teichoic acids and plays a key role in bacterial cell wall synthesis, which places it in the spotlight as a potential therapeutic target. The present work consists of a scientific paper on the structural elucidation of FmtA. Throughout this work, this protein is expressed, purified and crystallised to elucidate the structure by X-ray crystallography. Based on the diffraction data obtained, cycles of model building and refinement of the structural model of FmtA are carried out to analyse the structure of the protein and identify its most relevant aspects. This is a collaborative work with Prof. Dasantila Golemi-Kotra, from the Department of Biology at York University in Toronto (Canada). Previously, Prof. Golemi-Kotra determined a first crystal structure of FmtA at low resolution and in the absence of ligands. However, further structural studies where hampered by the irreproducibility of the protein crystals. The current work aims to reproduce the FmtA crystals to obtain higher-resolution diffraction data, allowing us to comprehend this target protein in more detail.

**KEY WORDS**: FmtA, *Staphylococcus aureus*, X-ray crystallography, protein purification, teichoic acids, penicillin-recognizing proteins

This project aligns with the **United Nations Sustainable Development Goals (SDGs)**, significantly contributing to SDG 3: Ensure healthy lives and promote well-being at all ages. The structural characterization of FmtA as a new therapeutic target has the potential to catalyse the development of new drugs, thereby safeguarding the well-being and health of people around the world. In particular, this work plays a crucial role in SDG 3 target 3.2, as it supports the development of effective drugs against Staphylococcus aureus, an infectious pathogen with global health implications, and the research contributes to preventing the spread of this pathogen and mitigating the associated health risks.

**AUTHOR**: Company Barber, Rebeca

**TUTOR**: Porcel Roldán, Rosa Caridad

**EXTERNAL COTUTOR**: Ramon Maiques, Santiago

Valencia, April 2024

**TÍTULO:** Caracterización estructural de FmtA: una nueva esterasa de *Staphylococcus aureus*.

**RESUMEN**: FmtA es una proteína reconocedora de penicilina con una función esterasa que consiste en hidrolizar el enlace éster que une la D-alanina a la cadena principal de los ácidos teicoicos. Se trata de una proteína de interés porque actúa sobre los ácidos teicoicos y desempeña un papel clave en la síntesis de la pared celular bacteriana, lo que la sitúa en el punto de mira como posible diana terapéutica. El presente trabajo consiste en la expresión, purificación y cristalización de esta proteína con el fin de obtener -mediante cristalografía de rayos X- datos estructurales que permitan la elucidación estructural de la proteína. A partir de los datos de difracción obtenidos, se llevan a cabo ciclos de modelado y refinamiento del modelo estructural de FmtA para analizar la estructura de la proteína e identificar sus aspectos más relevantes. Se trata de un trabajo en colaboración con la Prof. Dasantila Golemi-Kotra, del Departamento de Biología de la Universidad York de Toronto (Canadá). Anteriormente la Prof. Golemi-Kotra resolvió una primera estructura de FmtA libre de ligandos a baja resolución, pero no pudo continuar la caracterización estructural porque los cristales no eran reproducibles. El trabajo actual pretende reproducir los cristales de FmtA para obtener datos de difracción a mayor resolución que nos permitan una comprensión más detallada de esta proteína diana.

**PALABRAS CLAVE**: FmtA, *Staphylococcus aureus*, cristalografía de rayos X, purificación de proteínas, ácidos teicoicos, proteínas reconocedoras de penicilina

Este proyecto se alinea con los **Objetivos de Desarrollo Sostenible (ODS)** de las Naciones Unidas, contribuyendo significativamente al ODS 3: Garantizar una vida sana y promover el bienestar a todas las edades. La caracterización estructural de FmtA como nueva diana terapéutica tiene el potencial de catalizar el desarrollo de nuevos fármacos, salvaguardando así el bienestar y la salud de las personas en todo el mundo. En particular, este trabajo desempeña un papel crucial en la meta 3.2 del ODS 3, ya que apoya el desarrollo de fármacos eficaces contra el Staphylococcus aureus, un patógeno infeccioso con implicaciones para la salud mundial, y la investigación contribuye a prevenir la propagación de este patógeno y a mitigar los riesgos sanitarios asociados.

**AUTOR**: Company Barber, Rebeca

**TUTOR**: Porcel Roldán, Rosa Caridad

**COTUTOR EXTERNO**: Ramon Maiques, Santiago

Valencia, Abril 2024

# ACKNOWLEDGEMENTS

To the members of the Macromolecular Target Structures Unit, and especially to Santi, for his patience and dedication.

To my university classmates, for turning this stage into an unforgettable experience and for accompanying me throughout it.

To my mother for her unconditional support in all my adventures.

And finally, to all those who make the world of structural biology so fascinating. Your passion, dedication and contributions to this field of study are a great source of inspiration.

# INDEX OF CONTENTS

# INDEX OF FIGURES

# INDEX OF TABLES

# NOMENCLATURES AND ABBREVIATIONS

**3D:** Three-Dimensional

**Å:** Angstroms

**AU:** Absorbance Units

**CSS:** Complex Formation Significance Score

**Da:** Daltons

**D-ala:** D-alanine

**DNA:** Deoxyribonucleic Acid

**FPLC:** Fast-Performance Liquid Chromatography

**GlcNAc:** N-Acetyl Glucosamine

**IPTG:** Isopropyl-1-Thio-D-Galactopyranoside

**LB:** Luria Bertani

**LTA:** Lipoteichoic Acid

**MRSA:** Methicilin Resistant *Staphylococcus aureus*

**NGC:** Next Generation Chromatography

**PBP:** Penicillin-Binding Protein

**PBP2a:** Penicillin-Binding Protein 2a

**PBS:** Phosphate-Buffered Saline

**PDB:** Protein Data Bank

**PEG:** Polyethylene Glycol

**PRP:** Penicillin-Recognizing Protein

**rmsd:** Root Mean Square Deviation

**Rpm:** Revolutions Per Minute

**S:** Siemens

**SBDD:** Structure-Based Drug Design

**SDG:** United Nations Sustainable Development Goal

**SEC:** Size Exclusion Chromatography

**SSC*mec*:** Staphylococcal Cassette Chromosome *mec*

**SSM:** Secondary Structure Matching

**TA:** Teichoic Acid

**TB:** Terrific Broth

**VRSA:** Vancomycin-Resistant *Staphylococcus aureus*

**WT:** Wild Type

**WTA:** wall teichoic acid

# 1 INTRODUCTION

*Staphylococcus aureus* is considered one of the most widespread bacterial pathogens and a prevalent cause of mortality and morbidity worldwide. This Gram-positive bacterium of the Firmicutes phylum has long been recognized as a relevant human pathogen. Its colonization extends to human skin and mucosal surfaces, with the nasal cavity being its main reservoir (Kluytmans et al., 1997; Gorwitz et al., 2008). About 30% of the human population are *S. aureus* carriers, which lacks clinical manifestations but contributes to perpetuating its status as a notorious and widespread bacterial pathogen (Wertheim et al., 2005; Tasneem et al., 2022). *S. aureus* infections can originate from asymptomatic colonization or in the hospital setting by person-to-person transmission through direct skin-to-skin contact or due to infected fomites, making the pathogen a major cause of hospital and community-acquired infections (Guo et al., 2020; Cheung et al., 2021). This versatile pathogen is implicated in a wide spectrum of infections, ranging from uncomplicated skin infections to serious conditions such as pneumonia, sepsis, bacteremia, osteomyelitis, and endocarditis (Lowy, 1998; Guo et al., 2020; Cheung et al., 2021). *S. aureus* is characterized by a high intrinsic virulence (mediated by adhesive, host-cell damaging, and immunomodulatory molecules) and incredible genomic plasticity that allows it to adapt rapidly to different environmental conditions (Lee et al., 2018; Mlynarczyk-Bonikowska et al., 2022).

Its adaptability extends to antibiotic resistance. Despite being a pathogen naturally sensitive to most antibiotics, it has demonstrated a strong ability to evade the effect of antibiotics by acquiring various resistance mechanisms (Chambers and Deleo, 2009; Cheung et al., 2021). The acquisition of antibiotic resistance occurs through the selective elimination of susceptible microbes by the antibiotic, favouring the survival of those with diminished susceptibility. The primary causes of this phenomenon are the abusive use of antibiotics and the genomic plasticity of the bacteria (McCallum et al., 2006; Tasneem et al., 2022). The survival of *S. aureus* in the presence of antibiotics is attributed to various mechanisms, including specific mutations in existing bacterial genes with defined functions, the acquisition of exogenous resistance genes through horizontal gene transfer from other bacteria, and even tolerance to antibiotics through non-resistant but persistent cells (Grundmann et al., 2006; Balaban et al., 2019). In particular, Methicillin-Resistant *Staphylococcus aureus* (MRSA) has become a global health threat, as it is a major cause of bacterial infections, which are increasingly difficult to combat due to its emerging resistance to many of the current classes of antibiotics (Enright et al., 2002), including penicillins, cephalosporins, chloramphenicol, lincomycin, aminoglycosides, tetracyclines, macrolides, quinofurans, sulfonamides, and rifampicin, which considerably complicates its clinical management (Guo et al., 2020).

MRSA is a type of resistant "super bacteria" that is currently part of ESKAPE, a group of bacteria characterized by multidrug resistance (De Oliveira et al., 2020; Mlynarczyk-Bonikowska et al., 2022). Some studies suggest that the first resistant strains appeared before the introduction of methicillin in the mid-1940s, thus associating its emergence with the extensive use of penicillin. However, it was not until the 1960s that the first MRSA strain was reported (Lee et al., 2018). Since then, MRSA has spread globally, with infection rates increasing rapidly between the 1990s and early 2000s. Since 2005, a decline in some MRSA infections has been observed in the United States and Europe (Turner et al., 2019). Currently, MSRA is the most commonly identified antibiotic-resistant pathogen in many parts of the world, including Europe, the Americas, North Africa, the Middle East, and East Asia (Grundmann et al., 2006). However, differences in healthcare systems, infection prevention and control methods, or specific characteristics of circulating clones generate remarkable geographic variation (Figure 1), from the low prevalence in Northern Europe to the highest in some parts of America and Asia (Lee et al., 2018).

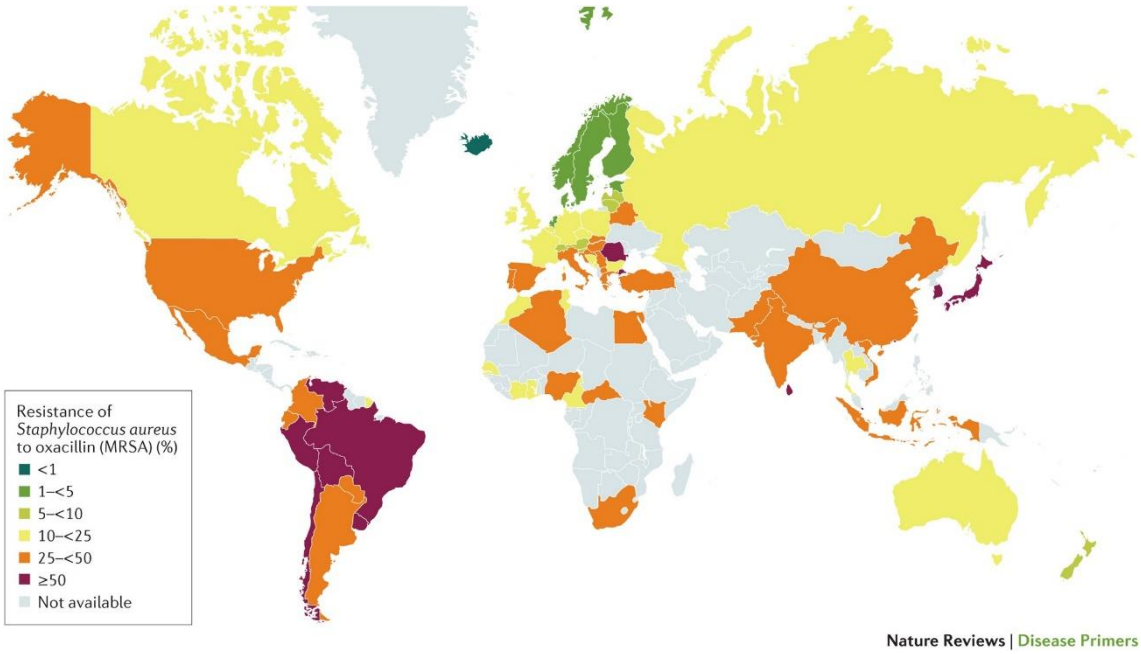


***Figure 1: Worldwide prevalence of MRSA.*** *World map showing the percentage of Methicillin-Resistant Staphylococcus aureus (MRSA) isolates by country. Data represented are adapted from the Center for Disease Dynamics, Economics & Policy Resistance Map. (Lee et al., 2018)*

MRSA represents a serious global health problem, and although its incidence has recently declined in some regions, it remains a major cause of serious bacterial infections (Turner et al., 2019). These infections are characterized by increased mortality, morbidity, virulence, invasiveness, and even biofilm formation, resulting in very severe infections that are difficult to treat and result in prolonged hospital stays (Cheung et al., 2021; Hashmi et al., 2023). Most MRSA infections are acquired nosocomially, as it is a pathogen that commonly emerges in hospitals and other healthcare settings, manifesting as complications of healthcare procedures or underlying conditions. Due to its common presence in healthcare settings where selective pressures for resistance are greatest, MRSA has adapted to these settings by developing resistance to multiple antibiotics (Grundmann et al., 2006; Chambers and Deleo, 2009).

Methicillin resistance is the most critical from a clinical point of view, as strains with such resistance are not susceptible to the most commonly used antibiotics: β-lactams (penicillins, cephalosporins, and carbapenems) (Grundmann et al., 2006). These antibiotics target penicillin-binding proteins (PBPs), key elements in cell wall biosynthesis, whose inhibition often results in bacterial cell death. PBPs are enzymes involved in peptidoglycan synthesis with different enzymatic activities (transpeptidase, transglycosylase, or carboxypeptidase). The β-lactam antibiotics covalently bind to them, acting as analogous substrates and inactivating the enzymes (Chambers, 1997). *S. aureus* exhibits different resistance mechanisms to β-lactam antibiotics, such as the synthesis of β-lactamases, mutations in PBP genes, or the synthesis of an additional PBPs (Mlynarczyk-Bonikowska et al., 2022). The latter is the most characteristic and relevant in MRSA, as a single element provides resistance to all β-lactam antibiotics: the staphylococcal cassette chromosome *mec* (SSC*mec*). SSC*mec* is a mobile genetic element (acquired by horizontal gene transfer) containing the *mecA* gene, which encodes penicillin-binding protein 2a (PBP2a), a peptidoglycan transpeptidase associated with methicillin resistance (Lee, et al., 2018). This enzyme has a low affinity for most β-lactam antibiotics, so it is unaffected by them and can take over cell wall biosynthesis while the four native PBPs of *S. aureus* (PBP1, PBP2, PPB3, and PBP4) are blocked (Grundmann et al., 2006; Lee et al., 2018).

Vancomycin has been the drug of choice for treating MRSA infections for many years. Vancomycin is a glycopeptide whose bactericidal effect inhibits cell wall synthesis. Its mechanism of action is based on its binding to the C-terminal D-alanyl-D-alanine of peptidoglycan precursors, blocking peptidoglycan polymerization (Chalmers and Wylam, 2020). However, *S. aureus* has also developed resistance mechanisms against vancomycin. This resistance is conferred by *van* genes, which modify the antibiotic target, synthesizing D-ala-D-lactate instead of D-ala-D-ala, thereby reducing vancomycin affinity (Tasneem et al., 2022). Strains with reduced susceptibility to vancomycin have been found in several countries (Utaida et al., 2003; Chalmers and Wylam, 2020) and have remained the antibiotic of last resort for treating severe MRSA infections, leading to the development of Vancomycin-Resistant *Staphylococcus aureus* strains (VRSA) (Cheung et et al., 2021). Although these resistant strains have not become widespread, they have further limited treatment options. This genetic adaptation is the most feared in *S. aureus* to date, creating a dire need to develop new compounds or antibiotics to treat *S. aureus* infection (Turner et al., 2019; Singh et al., 2022).

Antibiotics inhibiting cell wall biosynthesis, such as β-lactams and glycopeptides (e.g. vancomycin), are among the most efficient antibacterial agents for treating *S. aureus* infections. However, the emergence of resistance mechanisms has compromised their effectiveness, increasing the need to understand the cellular mechanisms of action and antibiotic resistance to develop new antibacterial compounds against *S. aureus* (Utaida et al., 2003). Recently, several novel antibiotics have been developed against MRSA, such as ceftaroline, ceftobiprole, dalbavancin, oritavancin, iclaprim, and delafloxacin, which are in different phases of clinical trials (Turner et al., 2019). An approach receiving increasing attention is multidrug therapy, as an appropriate combination of antibiotics confers benefits such as increased clinical efficacy or prevention of new resistance development (Chait et al., 2007; Lázár et al., 2022). Hashmi et al. (2023) evaluated the efficacy of the combination of three β-lactam drugs, meropenem, piperacillin, and tazobactam, compared to their use separately, resulting in a 41% reduction in bacterial cell growth. There is an urgent need to focus research on identifying new targets and developing new antibiotics against them. This requires a better understanding of essential bacterial processes such as cell wall formation, replication, translation, lipid biosynthesis, and interbacterial communication. Genomic and proteomic data are great tools for this purpose, as they allow the study of genes and proteins involved in different processes in *S. aureus*, which may provide new therapeutic targets (Utaida et al., 2003).

Recently, it has become of particular interest to reduce the resistance capacity of microorganisms and make them sensitive again to commonly used antibiotics (Hashmi et al., 2023). In particular, inhibiting non-essential genes involved in the synthesis of cell wall components can render MSRA susceptible to β-lactamases and vancomycin (Singh et al., 2022). Identifying novel methicillin resistance factors may be useful for designing new compounds and more effective antimicrobial strategies (Rajagopal et al., 2016). Generally, it is not a single gene or protein but the joint action of several of them that generates antibiotic resistance (McCallum et al., 2006). In *S. aureus*, several genes have been identified as factors associated with the level of resistance, such as *bla*, *fem*, *aux*, *llm*, *sigB*, *pbpB*, *sgtB*, *murZ*, *vraS*, or *fmt*. These factors are present in chromosomal DNA, outside the SSC*mec* element, and most are associated with peptidoglycan synthesis in the presence of methicillin (Komatsuzawa et al., 1999; Utaida et al., 2003). Several studies have shown that in the presence of cell wall active antibiotics, the gene expression pattern is altered, thus varying the expression of certain proteins. The set of genes that are affected comprises what is known as the cell wall stimulon, and the proteins they encode represent an important proteomic signature (Utaida et al., 2003; McCallum et al., 2006). In Utaida et al., 2003, transcriptional assays were analyzed to study the effect of cell wall inhibitory antibiotics (oxacillin, d-cycloserine, and bacitracin) on methicillin-susceptible strains. Each of the antibiotics was found to stimulate different cell wall-related genes. One of the proteins whose expression was affected was FmtA, which is in agreement with previous studies

such as those of Komatsuzawa et al., 1999, who reported that FmtA transcription is induced at high concentrations of oxacillin (β-lactam) and non-β-lactam cell wall inhibitors such as fosfomycin and bacitracin. FmtA is identified as a novel methicillin resistance factor of MRSA strains (Komatsuzawa et al., 1997), resistant to inactivation by β-lactams, as it exhibits low affinity for them, a slow rate of acyl-enzyme species formation and conformational changes in the presence of these antibiotics (Fan et al., 2007). Furthermore, FmtA is a central member of the cell wall stress stimulon (McAleese et al., 2006; Dalal et al., 2019), its expression increases in the presence of cell wall inhibitors and with the knockdown of genes involved in cell wall biosynthesis (Rahman et al., 2016). Inactivation of FmtA affects cell wall integrity, particularly the peptidoglycan structure (Komatsuzawa et al., 1999). Fan et al. (2007) demonstrated that FmtA exhibits high binding affinity to peptidoglycan in vitro and suggested that FmtA is involved in peptidoglycan biosynthesis under conditions of antibiotic-induced cell wall stress.

A key element of the cell wall of Staphylococcus aureus are teichoic acids (TAs) (Figure 2), they constitute 30-60% of the cell wall in gram-positive bacteria and play a crucial role in bacterial physiology, pathogenesis and antibiotic resistance, among others (Neuhaus and Baddiley, 2003; Brown et al., 2013). TAs are polymers consisting of a disaccharide linkage unit and a main chain composed of repeating ribitol or glycerolphosphate units linked by phosphodiester bonds (Lowy, 1998; Brown et al., 2013). A distinction is made between lipoteichoic acids (LTAs), which are anchored to the outer leaflet of the bacterial membrane, and wall teichoic acids (WTAs), which are covalently linked to cell wall peptidoglycan (Neuhaus and Baddiley, 2003; Brown et al., 2013). These polymeric chains can either be post-synthetically glycosylated by N-acetyl glucosamine (GlcNAc) or esterified by D-alanine (D-ala) (Neuhaus and Baddiley, 2003). For WTAs, alanine ester binding takes place extracellularly after the exportation of WTAs to the cell surface and is the way bacteria modulate their surface charge (Brown et al., 2013).

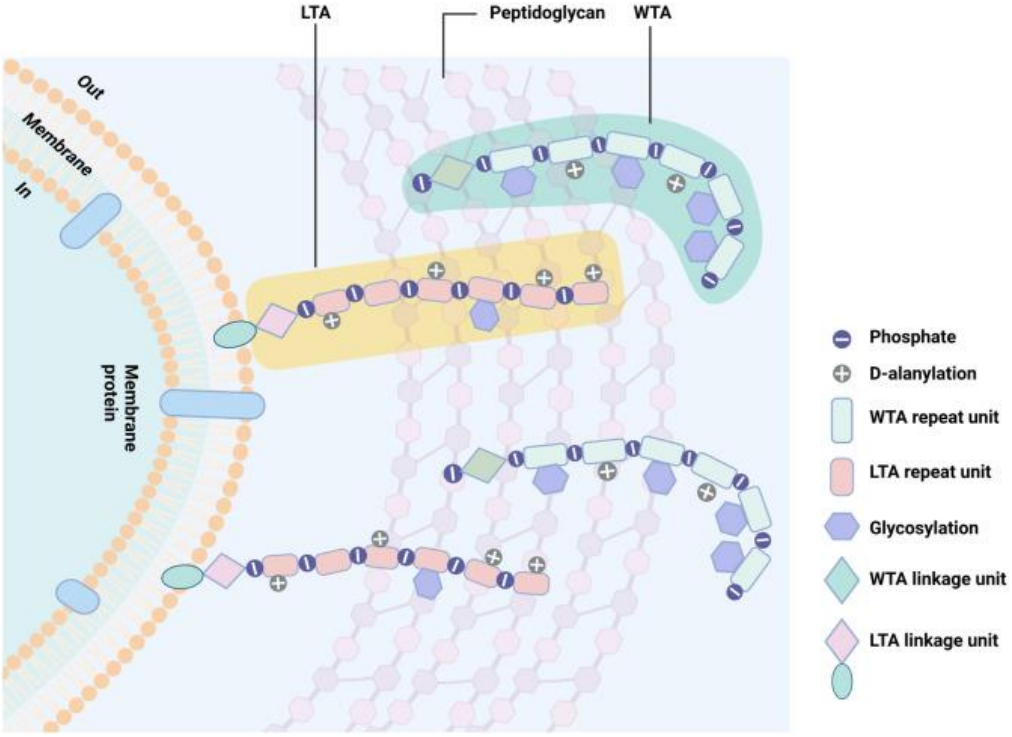


***Figure 2. Teichoic acids structure.*** *This diagram illustrates the structure of the Gram-positive bacterial cell wall, highlighting the presence and location of TA polymers in it. It delineates the two types of teichoic acids (WTA and LTA), depicting their respective positions, molecular structures and the possible modifications they undergo (Han et al., 2023).*

The D-alanine (D-ala) content of TAs plays a key role in modulating bacterial surface charge by introducing positive charges into the already negatively charged backbone of TAs. This gives TAs

a key role in several cellular processes, such as autolysis, adhesion, cation homeostasis, regulation of cell wall properties and resistance to certain antimicrobials (Collins et al., 2002; Neuhaus and Baddiley, 2003). The D-allyl content of TAs is environment-dependent and highly dynamic. D-alanyl ester substituents present on wall teichoic acids (WTA) are derived from those found on lipoteichoic acids (LTA); this conversion is a process known as D-alanyl turnover, which is enzymatically catalysed (Neuhaus and Baddiley, 2003). Rahman et al. (2016) and subsequently, Dalal et al. (2019) identified FmtA as one of the enzymes involved in this turnover process. Its function involves hydrolysis of the ester bond between D-ala and the carbon backbone of the TAs.

FmtA is part of the large family of proteins known as penicillin-recognising proteins (PRPs), which typically exhibit catalytic peptidase activity (Dalal et al., 2019). Within this family, FmtA belongs to the group of PBPs. As we have seen above, PBPs are proteins of great relevance as they are the main targets of β-lactam antibiotics (Chambers, 1997; Fan et al., 2007). PBPs are a group of proteins with great variability of catalytic activities and substrates, however, FmtA exhibits an esterase activity that is unique among PBPs. Furthermore, its core struture is the same as that of PBPs, although it has several structural differences (Fan et al., 2007; Dalal et al., 2019). In addition, it has a high level of sequence homology with other proteins of this family and retains some of the most conserved typical motifs as well as the hydrophobicity pattern (Komatsuzawa et al., 1997; Fan et al., 2007). There are several differences and similarities between FmtA and PBPs, but the most relevant commonalities for our work are that they are proteins involved in cell wall peptidoglycan biosynthesis, and that they covalently bind β-lactam antibiotics, and are strongly related to antibiotic resistance. The relevance of FmtA for the survival of Staphylococcus aureus and, in particular, its relationship with cell wall biosynthesis in the presence of antibiotic stress, make it a protein of great therapeutic interest for the treatment of antibiotic-resistant strains of S. aureus. To explore the potential of FmtA as a therapeutic target and understand its functions and mechanisms in detail, obtaining its macromolecular structure is essential (Dalal et al., 2019). The definition of a high-quality, high-resolution three-dimensional (3D) structure provides detailed information about the features and structural elements that are relevant to its functions and how they are involved. The structure provides an essential basis for structure-based drug design (SBDD), one of the most powerful and efficient processes in today's drug development landscape (Martin et al., 2024).

# 2 ANTECEDENTS

This work results from a collaborative effort with Prof. Dasantila Golemi-Kotra in the Department of Biology at York University in Toronto, Canada, who is a pioneer in the study of FmtA. In 2019, Prof. Golemi-Kotra, in collaboration with researchers from the Department of Biotechnology at the Indian Institute of Technology (IIT), successfully determined the crystal structure of *S. aureus* FmtA (Dalal et al 2019). This groundbreaking achievement marked the first atomic structure of FmtA, offering a glimpse of the protein at a limited resolution of 2.58 Å, and in the absence of ligands. To delve deeper into the understanding of the protein's active site and rationally design specific inhibitors, higher resolution structural information about the protein and its complex with substrates was needed. Unfortunately, reproducing the protein crystals proved challenging despite numerous attempts, and the project and the collaboration slowly languished. Then, in 2022, during a congress in Toronto, Santiago Ramón-Maiques and Prof. Golemi-Kotra decided to revive the study on the structural and functional characterization of FmtA.

# 3 OBJECTIVES

The primary objective of this collaborative study is to reproduce the crystals of FmtA and determine its three-dimensional structure with higher resolution than previously reported in Dalal et al., 2019.

To accomplish this aim, the following sub-objectives were established:

1. Express and purify the FmtA protein from *S. aureus* in sufficient quantity and purity to attain crystallization.
2. Obtain high-quality diffraction crystals for structural determination.
3. Perform X-ray diffraction experiments using synchrotron radiation.
4. Build and refine the 3D model of FmtA.
5. Analyze the FmtA structure and identify its most relevant aspects.

This project aligns with the United Nations Sustainable Development Goals (SDGs), significantly contributing to SDG 3: Ensure healthy lives and promote well-being at all ages. The structural characterization of FmtA as a new therapeutic target has the potential to catalyse the development of new drugs, thereby safeguarding the well-being and health of people around the world. In particular, this work plays a crucial role in SDG3 target 3.2, as it supports the development of effective drugs against Staphylococcus aureus, an infectious pathogen with global health implications, and the research contributes to preventing the spread of this pathogen and mitigating the associated health risks.

# 4 MATERIALS AND METHODS

## 4.1 FMTA EXPRESSION

The FmtA wild-type (WT) protein and a variant bearing the point mutation S127A were expressed in bacteria, as previously reported by Prof. Golemi-Kotra (Fan et al., 2007). The DNA expression vector encoding FmtA-WT and FmtA-S127A were obtained from Prof. Golemi-Kotra. These pET24a vectors (Novagen) encoded an N-terminal truncated version of the FmtA, spanning residues 43–397.

For bacterial transfection, 2 µl of the expression plasmid were added to 50 µl of chemically competent BL21 (DE3) pLysS *Escherichia coli* cells (Invitrogen) and gently mixed. Following a 30 min incubation on ice, the sample was heated at 42 °C for 45 sec and placed on ice for 2 min. To allow the expression of antibiotic resistance, the cells were complemented with 250 µl of Luria Bertani (LB) broth media and incubated for 1 h at 37 °C in a shaking incubator. 50 µl or 200 µl of the culture were spread with a metal handle on Petri dishes with LB-agar solid media supplemented with 50 µg/ml kanamycin and 34 µg/ml chloramphenicol and incubated overnight at 37 °C.

For protein expression, a single transformant colony was picked with a wire loop and inoculated in an Erlenmeyer with 25 ml liquid LB supplemented with kanamycin and chloramphenicol and cultured in an orbital shaker overnight at 37 °C. On the following day, 10 ml of the pre-culture were inoculated in 1 L of Terrific Broth (TB) medium (Sambrook and Russell, 2001, A2.4) supplemented with 50 µg/ml kanamycin, 34 µg/ml chloramphenicol, 0,4 M sorbitol, and 2,5 mM betaine. The culture was grown in a shaking incubator at 37 °C and 180 rpm for approximately 5 h until it reached an optical density at 600 nm of 0.6 (~5 h). Protein expression was induced by the addition of 1 mM isopropyl-1-thio-D-galactopyranoside (IPTG). Subsequently, the cell culture was shaken at 22 °C overnight. Cells were harvested by centrifugation at 6.000 rpm and

15 °C for 30 min. To eliminate the growth media, the cells were resuspended in 20 ml phosphate-buffered saline (PBS) and harvested by centrifugation. Upon removal of the supernatant, the cell paste was kept frozen at -80 °C. The expression protocol was the same for FmtA WT and S127A mutant.

## 4.2 FMTA PURIFICATION

FmtA WT and S127A were purified by two consecutive chromatographic steps, a cation exchange chromatography and size exclusion chromatography (SEC), as previously reported (Dalal et al., 2021). Briefly, the cell paste from 1 L bacterial culture was resuspended in 40 ml of buffer A (50 mM sodium phosphate pH 7.2) supplemented with 1 mM Pefabloc (Sigma) protease inhibitor and disrupted by sonication. The lysate was clarified by centrifugation at 15.000 rpm for 30 min.

The clarified supernatant was filtered through a 0.45 um syringe filter and loaded with a peristaltic pump onto a HiTrap SP FF 5ml column (Cytiva) equilibrated in buffer A. The column was connected to a fast-performance liquid chromatography (FPLC) NGC (Next Generation Chromatography) system (Bio-Rad) and washed with buffer A supplemented with 250 mM NaCl. The protein was eluted from the column increasing the salt in buffer A to 1 M in a linear gradient of 10 column volumes. The fractions collected during protein elution were analyzed by SDS-PAGE using a discontinuous gel of 4% and 15% acrylamide, and stained with Coomassie. Those fractions showing higher amounts of a band of the expected molecular weight of FmtA (~40 kDa) were pooled and concentrated down to ~2 ml using an Amicon Ultra 30 kDa - 10 ml centrifugal device (Millipore). The sample was subsequently purified through a Superdex 200 increase 10/300 size exclusion chromatography column (Cytiva) equilibrated in buffer A. The column was connected to an NGC system and operated at a constant flow of 0.5 ml/min. The sample was applied in 3 different injections of ~0.7 ml and collected in 0,5 ml fractions. As before, fractions were analyzed by SDS-PAGE. Fractions showing the expected FmtA band were pooled and concentrated first with an Amicon Ultra15 30 kDa - 10 ml Centrifugal Filter to ~1 ml and then on a Vivaspin 2 ml Centrifugal Concentrator (Sartorius) until a final volume of ~100 µl.

All purification steps were carried out at 4 °C to enhance protein stability and decrease degradation by bacterial proteases. Protein concentration was determined by the Bradford method using the Bio-Rad protein assay reactive (Bio-Rad) and using bovine serum albumin (Sigma) for the standard protein curve. Alternatively, protein concentration was measured by absorbance at 280 nm using a nanophotometer NP80 (Implen) and a theoretical extinction coefficient value of 56.160 $M^{-1}cm^{-1}$ calculated from the primary FmtA sequence with the ProtParam tool (Gasteiger et al., 2005).

## 4.3 FMTA CRYSTALLIZATION

Crystallization was performed at room temperature using the hanging-drop vapor diffusion method in 24-well plates (Hampton Research). Drops consisting of 1.5 µl protein solution plus 1.5 µl reservoir solution were equilibrated against 1 ml of reservoir solution. The reservoir solution contained 0.1 M Tris-HCl pH 8.5, 0.2 M NaCl and polyethylene glycol (PEG) 3350 at concentrations between 23 and 28% (w/v) as were previously reported (Dalal et al., 2019).

FmtA-WT was crystallized at 26,9 mg/ml, whereas FmtA-S127A was crystallized at concentrations between 12 and 41 mg/ml. Also, the proteins were co-crystallized with 27 or 50 mM ampicillin and 25 or 50 mM ribitol, using the described conditions.

All crystals were cryoprotected by briefly soaking in the reservoir solution with 5% increments in the PEG concentration, up to 35%. In the case of co-crystallization with ampicillin or ribitol, the ligands were also added to the cryo-solution. The crystals were fished using a cryo-loop similar in size to the crystal and rapidly flash-frozen in liquid nitrogen.

## 4.4 DATA COLLECTION AND STRUCTURE DETERMINATION

The frozen protein crystals were shipped under liquid nitrogen temperature in a dry-shipper dewar to the beamlines for macromolecular X-ray diffraction at ALBA (Barcelona) or ESRF (Grenoble) synchrotrons. The X-ray diffraction experiments were performed remotely from Valencia using dedicated software to operate the experimental hutch at the beamlines. Multiple X-ray diffraction datasets were collected from single protein crystals at 100 K temperature and using Pilatus 6M detectors (DECTRIS). The experiment collected a ~180° oscillation of the crystal in approximately 3–5 min, generating large amounts of diffraction data that were automatically processed, indexed and scaled at the synchrotron computational clusters using Autoproc (Vonrhein et al., 2011). The best diffraction datasets regarding resolution limit and intensity were chosen based on the data collection statistics. Crystallographic phases were obtained by molecular replacement using the reported human FmtA structure (Dalal et al., 2019 ; PDB ID: 5ZH8) as the search model and the program Phaser implemented in the CCP4 v8.0 (Collaborative Computational Project Number 4 in Protein Crystallography) suite (Agirre et al., 2023). The FmtA-WT model was constructed on personal computers by iterative cycles of manual model building using *Coot* 0.9.8.1 (Crystallographic Object-Oriented Toolkit) (Emsley et al., 2010) and refinement with Refmac5 (Vagin et al., 2004) in CCP4 and Phenix 1.20.1 (Python-based Hierarchical Environment for Integrated Xtallography) (Liebschner et al., 2019). The structure analysis was done with Coot and PyMOL (The PyMOL Molecular Graphics System, Version 3.0 Schrödinger, LLC.), and all 3D figures were prepared with PyMOL. Superpositions were done with COOT using the secondary structure matching (SSM) algorithm. The interface between subunits was analyzed by PDBePISA (Protein, Interfaces, Surfaces and Assemblies) tool (Krissinel & Henrick, 2007).

# 5 RESULTS AND DISCUSSION

## 5.1 EXPRESSION AND PURIFICATION OF FMTA

To reproduce and improve the quality and resolution of FmtA structural data by X-ray crystallography, the initial step involved producing substantial quantities of pure and homogeneous protein. At the beginning of this project, this task was done by Prof. Golemi-Kotra, who shipped the frozen protein from Canada for our initial crystallization attempts. Unfortunately, custom restrictions often resulted in considerable paperwork, prolonged delays, and the arrival of samples unfrozen and partially precipitated. For this reason, we asked Prof. Golemi-Kotra for the FmtA expression vectors and set up the protocols for the expression and purification of FmtA in our laboratory.

To obtain the large amounts of FmtA required for X-ray crystallography, the WT and S127A mutant were expressed separately in BL21 pLys'S competent cells. Transformed cells were cultured on LB plates supplemented with antibiotics, and only a few colonies were obtained. This low efficiency in the transformation was likely due to the low concentration of the DNA plasmid.

However, these colonies were adequate to continue the pre-culture and culture process. Once inoculated in TB, the bacteria took about 5 h to reach the absorbance required for IPTG induction at low temperatures and were then left to grow overnight. The expression of the recombinant protein was successful, as shown below for the purification results.

To purify FmtA, we lysated the producing bacteria by sonication, clarified the supernatant by centrifugation and performed a cation exchange chromatography (Figure 3A). The elution from the column, monitored by absorbance at 280 nm, showed that after sample loading, a first peak appeared, corresponding to the proteins that did not bind to the column (Flow-trough, F). Then, a second peak appeared upon washing the protein with 0.25 M salt, corresponding to 25% of

buffer B. Finally, during a salt gradient to 100% of buffer B, corresponding to 1 M salt, a third large and sharp peak appeared between 6 and 38 ml (fractions 9 to 27). This peak reached the maximum absorbance at 25 ml after the start of the gradient. Although we did not make a band identification, we deduced that the third peak corresponded to the elution of the protein of interest, which was overexpressed. Also, the profile of the peak and the elution volume were similar to those reported by our collaborators.

Throughout the purification process, samples of lysate (L), supernatant (S), flowthrough (F), and column wash (W) were taken and loaded onto an SDS-PAGE to monitor that the protein was correctly expressed and purified without losses during the chromatography. In addition, to select the fractions with the protein for the next chromatographic step and to check the purity, we load those fractions of the peak (Figure 3B) on de SDS-PAGE. It was estimated that about 5 µg of protein were loaded in each well. The result of the SDS-PAGE stained with Coomassie was bizarre. Rather than observe a band at the expected size of 41.3 kDa for the FmtA construct, we observed a thick protein smear in the region delimited by the 40 and 80 kDa markers. This smear was barely seen in the fractions not retained by the column (such as flowthrough and column wash), suggesting that the smear corresponded to our protein of interest.

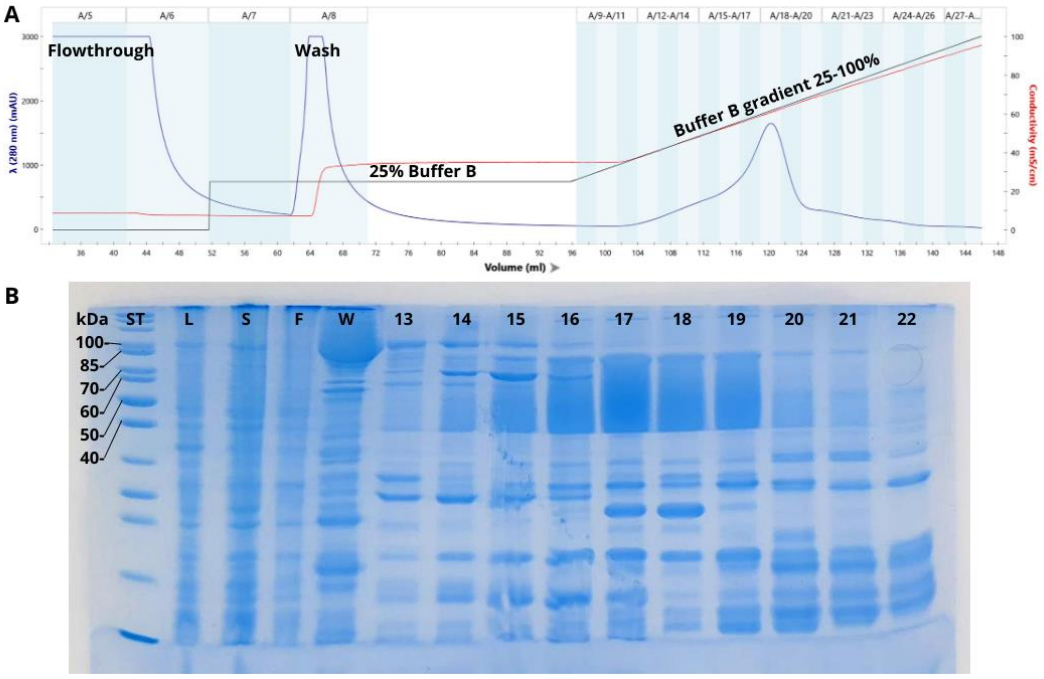


***Figure 3. Cation exchange chromatography results.*** *A. Chromatogram of ion exchange chromatography. The X-axis shows the elution volume (ml) at the bottom and the collected fractions at the top. The Y-axis shows the percentage of buffer B (black), the conductivity (red, mS/cm) and the absorbance at 280nm (blue, mAU). B. 4-15% SDS-PAGE of the purification steps: molecular weight standards (St); lysate (L); supernatant (S); flow-through (F); column wash (W) and fractions 13 to 22 (13-22).*

Revising the literature, we found studies that had already described this phenomenon for FmtA (Fan et al., 2007). Based on these studies, the smear is characteristic of FmtA that, in reducing and denaturing conditions, behaves as a mixture of monomer (40 kDa) and dimer (80 kDa). This dimer appears despite reducing conditions, and therefore, it does not depend on the formation of disulfide bridges between cysteines. According to Fan et al. (2007) studies, FmtA behaves as a monomer under physiological conditions, with the expected molecular mass of 43 kDa, as calculated from size exclusion chromatography analysis. The dimer observed in SDS-PAGE is an artifact formed by partial denaturation with the SDS and the formation of non-covalent interactions between exposed hydrophobic patches of the protein.

As shown in Figure 4A, the elution profile of the gel filtration step (only one of the three chromatograms obtained is shown, as they are all identical) showed that the protein eluted in a large, sharp, high peak in the elution volume between 18-21 ml, with the maximum absorbance at 19 ml. Furthermore, the fact that this is the only peak and that there is no absorbance signal before it indicates that no protein aggregates have formed (if they had, the signal would appear after the dead volume of the column). According to the calibration of the standard column, the position of this peak coincided with the expected molecular mass of FmtA as a dimer.

We ran the collected fractions potentially containing FmtA onto a 4-15% SDS-PAGE, together with a sample before the gel-filtration, to assess the purity of the sample eluting in the peak (Figure 4B). The gel, stained with Coomassie, showed that most of the contaminants were eliminated in this chromatographic step. Fractions 23–28, which contained the protein of interest and few contaminants, were selected, pooled and concentrated. The maximum protein concentration obtained in the gel filtration buffer was 41 mg/ml, which we considered sufficient to attempt the crystallisation.

To obtain crystals suitable for X-ray crystallography, the protein must reach a supersaturation (the highest concentration possible without causing aggregation or precipitation) of between 2-50 mg/ml; it must also be as close to homogeneous as possible, which is key to obtaining crystals that diffract at high resolution (Dessau and Modis, 2011). As our protein solution was at a high concentration and did not contain many contaminants, we decided it was ready to attempt the crystallization.

The results of the purification of S127A are not shown; they are very similar to those of WT, as the mutation does not affect the stability and solubility of the protein.

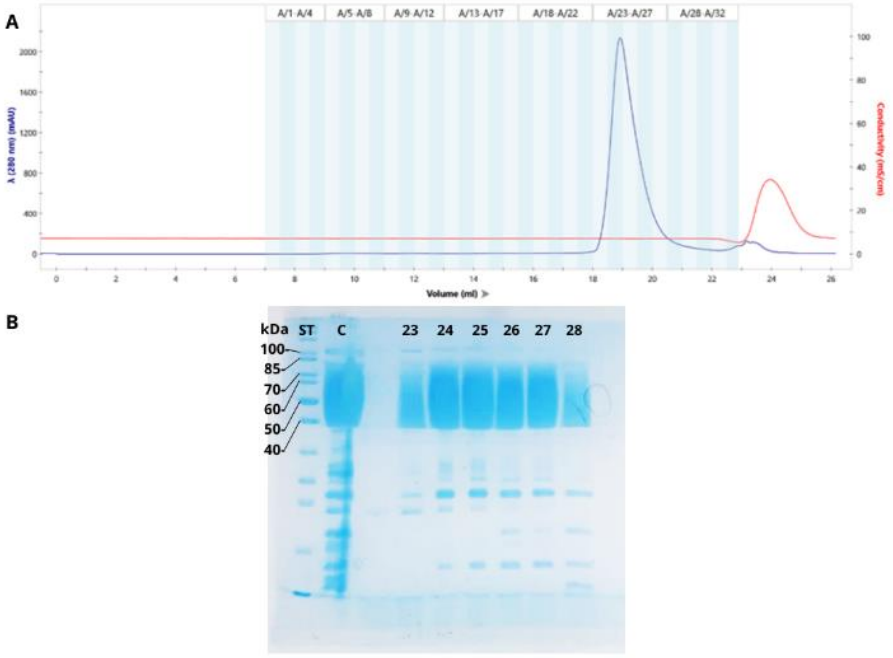


***Figure 4. SEC purification results.*** *A. Chromatogram of size exclusion chromatography. The X-axis shows the elution volume at the bottom and the collected fractions at the top. The Y-axis shows the percentage of buffer B in the gradient (black), the conductivity (red, mS/cm) and the absorbance at 280nm (blue, mAU). B. 4-15% SDS-PAGE of the purification steps: molecular weight standards (St); concentrate (C) and fractions 22 to 28 (22-28).*

## 5.2 FMTA CRYSTALLIZATION AND DATA COLLECTION

A major problem encountered by Prof. Golemi-Kotra and collaborators was the inability to reproduce FmtA crystals. In turn, our efforts to purify the protein and grow crystals proved successful. Indeed, we found that the purified FmtA sample exhibited a propensity to crystallize

readily. Whether utilizing the protein initially sent by Prof. Golemi-Kotra or the protein expressed and purified by us, the crystals appeared 24 h after setting up the crystallization plates (Figure 5, Figure 6A). The crystals, although small, continued growing and reached a maximum size of approximately 0.2–0.3 mm in one week. The best crystallization drops showed few large crystals and were obtained using as reservoir solution 100 mM Tris-HCl pH 8.5, 23-25% PEG 3350, and 200–400 mM NaCl. These conditions were similar to those defined in Dalal et al. (2019), but they reported that the crystals required 3 months to appear.

The best unique crystals were harvested using cryo-loops (Figure 6B), transferred to cryo-solutions, and flash-cooled in liquid nitrogen. The cryo-solutions, in this case consisting of increasing the PEG concentration in the reservoir condition to 30–35%, are needed to prevent the formation of ice crystals that interfere with the protein diffraction. For some crystals, we included ampicillin or ribitol in the cryo-solutions to favor the soaking into the active site of the proteins forming the crystal to obtain the structure of the complex with these ligands. In general, the crystals appeared fragile, and they often broke or dissolved during the transfer to the cryo-solutions and during the fishing process.

***Figure 5. FmtA crystals.*** *FmtA crystals of different morphologies obtained by the hanging drop and vapour diffusion technique. The dimension of the largest crystals is about 0.3 mm. Some of them are small (left), others show branching (centre) and others are large aggregates formed by other smaller crystals (right).*

The crystals frozen in a loop were shipped to the beamlines for macromolecular X-ray diffraction at the synchrotrons ALBA (Barcelona) and ESRF (Grenoble). We then performed diffraction experiments using the high-energy X-rays produced by the particle accelerator and collecting the diffraction pattern in state-to-the-art detectors (Figure 6C). These X-ray diffraction patterns give us indirect information about the molecules packed into the diffracted crystal. All the diffraction spots must be indexed, scaled and merged with complex mathematical calculations that, fortunately, are automatically done at the synchrotron computational cluster, obtaining reflection data (Figure 6D).

After a careful analysis of the statistics for all the data sets collected, we chose that of the crystal named "B2X11" for being of higher quality and having higher resolution information. Crystal B2X11 corresponded to FmtA WT without soaking any ligand, that is, in the APO form. B2X11 diffracted X-rays to a resolution of 2.149 Å, exceeding the resolution limit obtained by Dalal et al. (2019), which was 2.58 Å. This improved resolution limit indicates the minimum distance we will find between distinguishable atoms and although seemingly small, it provided a large amount of information to improve the quality of the three-dimensional model of FmtA. In addition to the resolution, there are other relevant parameters on the quality of the crystal, as shown in Table 1.

We highlight some aspects of these parameters. The ratio between the mean of the reflection intensities and their standard deviation is a signal-to-noise ratio. A value < 1.0 in the highest resolution shell, which is the area of the detector that collects the reflections with high resolution information, indicates that the detection is noisy and useless. The $R_{merge}$ is a

correlation factor that measures the precision of the intensities, or the dispersion between individual measurements of equivalent reflections. An $R_{merge}$ value of less than 4% corresponds to an accurate data set (Wlodawer et al., 2007). The completeness is a measure of the coverage of all theoretically possible reflections, and is typically somewhat lower in the highest resolution shell, where the high-resolution reflection data may not be 100% complete (Wlodawer et al., 2007).

Overall, and although we focuses our work on crystal B2X11, it is important to remark that most of crystal produced X-ray diffraction datasets of good quality that could be used to solve the structure of the protein.

***Table 1. Statistics for diffraction dataset.***

| | Overall | Inner Shell | Outer Shell |
|---|---|---|---|
| Low resolution limit | 64.654 | 64.654 | 2.058 |
| High resolution limit | 1.932 | 5.705 | 1.932 |
| | | | |
| Rmerge (all I+ & I-) | 0.054 | 0.024 | 1.246 |
| Rmeas (all I+ & I-) | 0.059 | 0.026 | 1.350 |
| Rpim (all I+ & I-) | 0.023 | 0.010 | 0.514 |
| Total number of observations | 306147 | 14372 | 15236 |
| Total number unique | 45263 | 2262 | 2264 |
| Mean(I)/sd(I) | 18.1 | 57.1 | 1.4 |
| Completeness (spherical) | 83.3 | 99.9 | 24.4 |
| Completeness (ellipsoidal) | 94.7 | 99.9 | 61.9 |
| Multiplicity | 6.8 | 6.4 | 6.7 |
| CC(1/2) | 0.999 | 0.999 | 0.610 |

## 5.3 STRUCTURE DETERMINATION OF FMTA

Each reflection in X-ray crystallography is characterised by its position, amplitude and phase. However, when collecting diffraction data, only the position and intensities of the reflections are directly measured, not the phases, and this creates the so-called "phase problem". In our case, we solved the problem using a molecular replacement method. This consists of using the already published lower-quality FmtA structure (Dalal et al., 2019; PDB ID: 5ZH8) as a search model to estimate the missing phases. Subsequently, electron density maps (Figure 6E) were generated from the experimental reflection data and the estimated phases. These maps indicate the path of the polypeptide chain, and with the resolution obtained, also show the orientation of the amino acid side chains.

The next step, known as "model building", consisted in adjusting the initial FmtA model model in the electron density maps, removing from the model those parts that do not fit in the electron density maps, and adding and repositioning others according to the electron density demand. During these manual modelling, we had to take into account other considerations, such as the stereochemical constraints, angular conformations, the nature and polarity of nearby residues or the presence of hydrogen bonds or other interactions. After manual building, we further refined the model with an automatic program (Refmac in CCP4 or Phenix), that in addition to try to improve the geometry of the model and the fitting to the electron density maps, also refines other factors, such as the vibration of the atoms (temperature or B-factors) and their occupancy. Then, we used the improved model to estimate new crytsallographic phases, that combined with the experiment data should result in an improved electron density map with more information to continue constructing the model. In summary, we employed an iterative method of manual building and automatic refinement, and after 15 cycles, we obtained the best model that could not be improved any further (Figure 6 G).

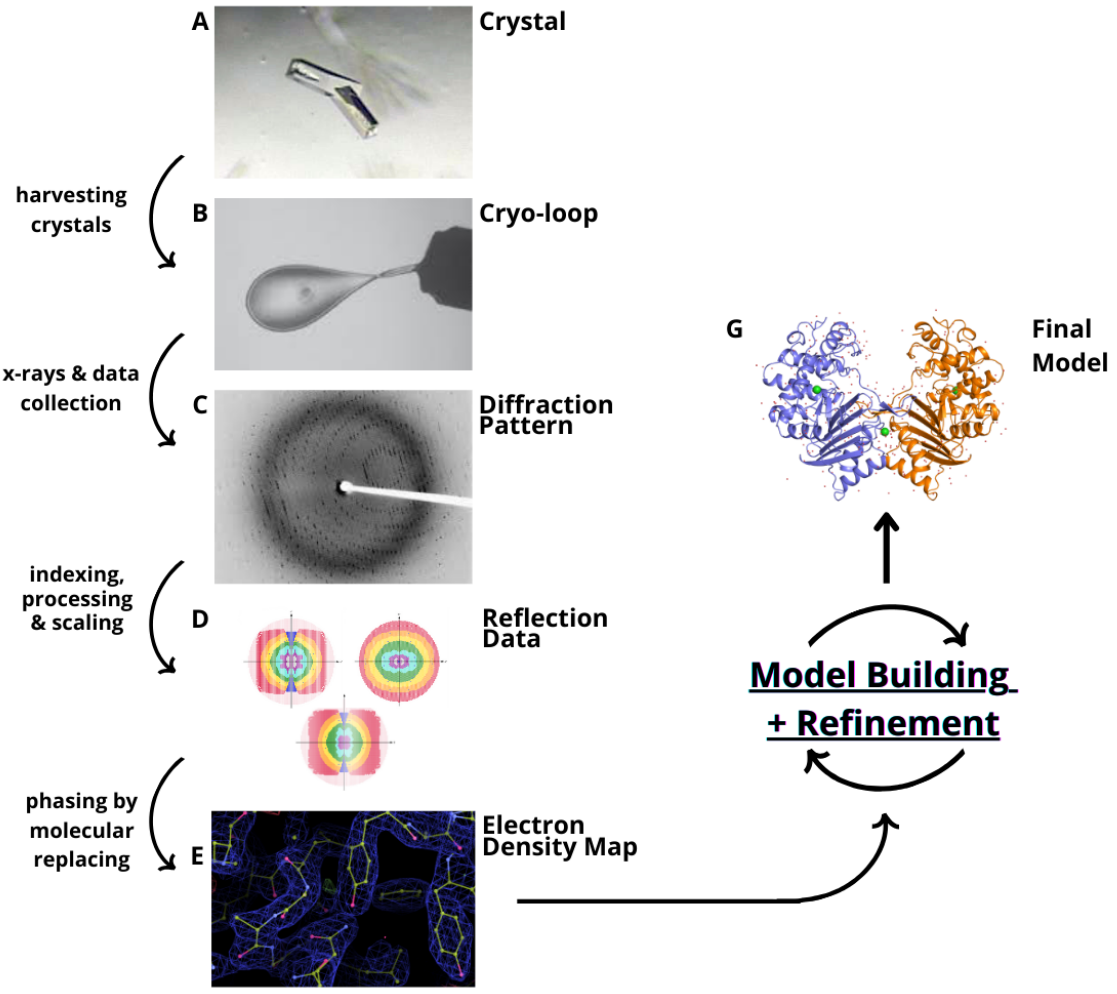


***Figure 6. Data collection and structure determination flowchart.*** *A. A frozen crystal is obtained throughout the crystallization process. B. A harvested crystal using cryo-loops for synchrotron shipment. C. The diffraction pattern captured by the synchrotron detector, as a result of exposing the crystal to X-rays. D. Reflection data obtained after scaling, processing, and indexing the raw data of the diffraction pattern. E. Electron density map crafted by the experimental data and crystallographic phases obtained from a model. F. The final model of the FmtA structure derived from the whole process.*

After each iterative cycle of modelling and refinement, the crystallographic values $R_{work}$ (or $R_{factor}$) and $R_{free}$ were checked, which are indicators of the quality of the being refined. The $R_{work}$ is an indicator of the correlation between the molecular model and the experimental diffraction data. However, this factor can be misleading and give a good value even if the model has misinterpreted the data. That is why $R_{free}$ becomes interesting, as it is similar to $R_{work}$ but uses a 5% of the total reflections that were not used during refinement and thus, is not model-biased. During the refinement, we monitored that both $R_{work}$ and $R_{free}$ decrease in parallel, and do not separate more than 6%, as this could indicate mistakes in the protein model.

Figure 7 shows the evolution of these statistics throughout the cycles of model construction and refinement. It is observed that during the first cycles, there is a drastic decrease in both values, because more noticeable and evident changes are made during these cycles that substantially improve the correlation of our model with the experimental data. After refinement cycles 8 and 9, this improvement is less evident, even leading to a slight increase in the statistics, in addition to their separation. It was at this point that the decision was made to switch refinement programs (from Refmac5 to Phenix). The process was stopped when both statistical values ceased to improve significantly after further iterative cycles.

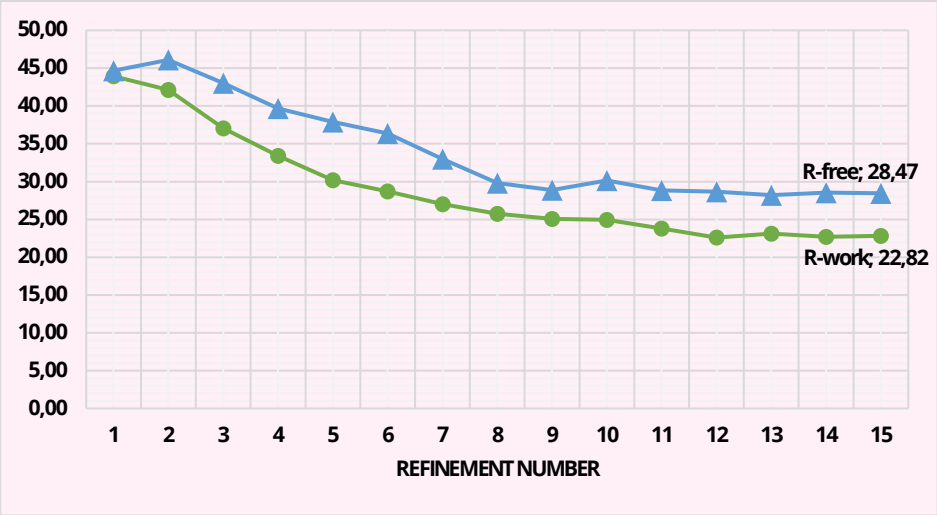


***Figure 7. $R_{work}$ (green) and $R_{free}$ (blue) values throughout the 15 cycles.*** *The X axis show the refinement cycle number, and the Y axis the Rs values. This figure also shows the last values (the values obtained after the 15$^{th}$ cycle) for both $R_{work}$ and $R_{free}$.*

In the study conducted by Read et al. (2011), the authors aimed to establish a relative rank or percentile for a structure's score, enabling it to serve as a metric for comparative quality. The methodology estimated the ratio between the $R_{free}$ and the resolution of all existing protein structures in the Protein Data Bank (PDB) up to that point. According to the findings, the study suggests that for most protein crystal structures determined at a resolution of 2,149 Å, a $R_{free}$ value close to 24 % would correspond to a favorable percentile. However, in the case of our protein, the observed $R_{free}$ was 28.47, indicating a lower quality compared to the majority of PDB proteins solved at a similar resolution. Despite this, we do not consider our model to be of poor quality for its resolution, as during the model building and refinement cycles, the model fitted well to the electron density maps. It has been deduced that this high $R_{free}$ value may be since a large part of our protein model (subunit B, see below) appears more flexible, likely due to decreased contacts within the crystal lattice. This means that the model for part of the protein (subunit A) is of high quality as expected for a protein crystal diffracting at this resolution, whereas the definition of the other part (subunit B) is poorer.

Once we decided to stop refining the model due to no significant improvements, we turned our attention to studying the FmtA structural model obtained. We compared our findings with those of Dalal et al., 2019, to understand our contributions to FmtA's structural analysis.

Our final model is shown in Figure 8, where we observe 2 chains (A and B), 300 water molecules and 3 chlorine atoms. These chlorines were not described by Dalal et al. (2019) and do not appear as part of the current PDB structure, but due to their position in both subunits and especially on the contact surface between them, they seem to have a relevant structural role. We observe several α-helices, β-sheets and loops. A very distinctive and striking feature of the structure is the large pocket formed between the two chains, which is probably responsible for holding the substrate during catalysis, as we will discuss below.

The complete sequence of FmtA consists of 794 residues (397 on each chain). Based on the construction used, our model would ideally show all the amino acids in each chain starting from residue 42, but chain A consists of 353 amino acids from Leu45 to Gln397 and chain B of 352 amino acids from Ser46 to Gln397. The lack of these amino acids in the model may be because the N-terminal region is flexible. It is important to remark that the electron density shows the average of all the protein molecules in the crystal, and thus, if a particular region adopts a flexible conformation, it would not be visible in the model because the average electron density for this part would be weak.

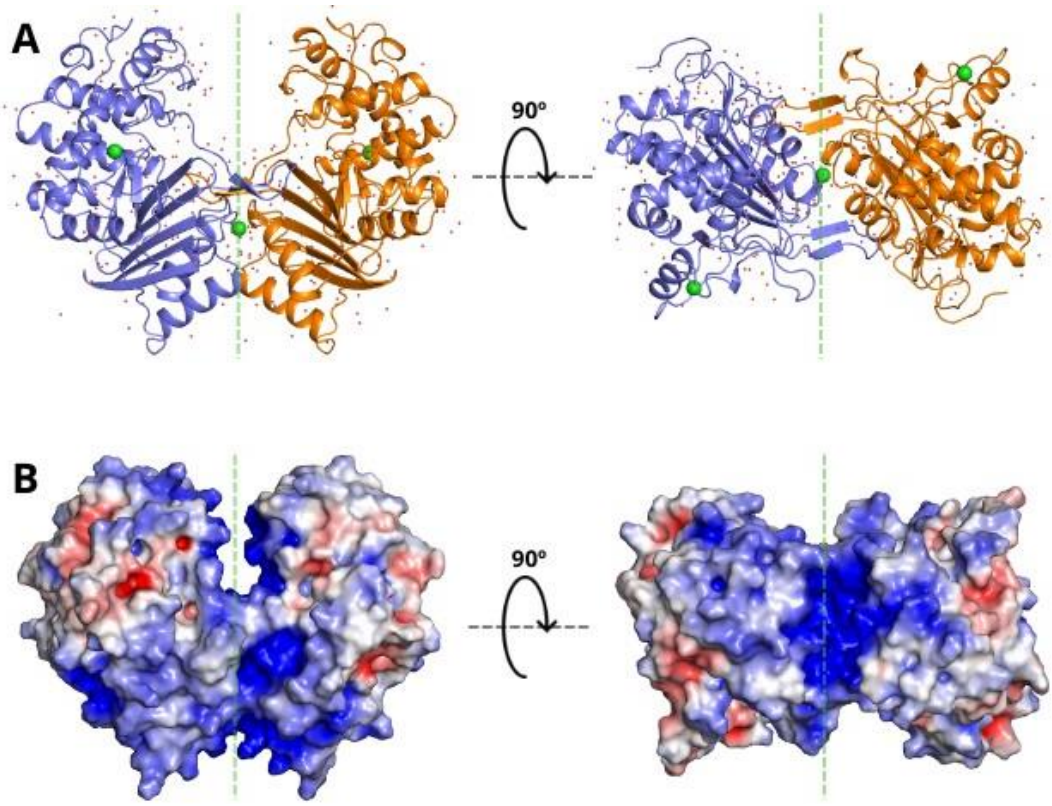


***Figure 8. Final model structure and surface charge distribution.*** *A. Cartoon representation of the final model. The structural model of FmtA consists of two subunits A (blue) and B (orange), as well as 300 water molecules (red spheres) and 3 chlorine atoms (green spheres). The axes of symmetry are marked with green dotted lines. On the symmetry axis between both chains we find a chlorine and the dimerization surface. B. Surface charge distribution of FmtA. The surface of FmtA is mostly positive, except for some external regions exposed to the solvent. There is a large positively charged pocket, that is solvent exposed and corresponds with an enlarged active that complements the negatively charged backbone of WTA.*

We have resolved the FmtA structure as a dimer, composed by A and B subunits. The structure of the two subunits within the asymmetric unit was highly similar, as indicated by the root mean square deviation (rmsd) of 0.6 Å for superposition of 345 C- α atoms in the polypeptide chain of both subunits. This superposition (shown on Figure 9A) excluded the N-terminal residue 45 and residues 203 to 208 that could not be modeled in the structure of subunit B. Indeed, the modeling and refinement of the B subunit was more difficult because the electron density was less well-defined, possibly due greater flexibility caused by less inter-protein contacts within the crystal lattice.

Figure 9B compares the secondary structures of the A and B chains of our model with each other and with the ones on the PDB 5ZH8 model. As defined by Dalal et al., 2019 in their model, each FmtA chain consists of 14 α-helices, 15 β-sheets and many loops. However, in our model, we only identified 12 α-helices and 10 β-sheets. This may seem like a big difference, but it is to be expected in the case of secondary structures consisting of very few residues (α-helices of 3 to 5 residues and β-sheets of 3 residues or even 2 residues), which makes a small deviation in a side chain cast doubt on the presence of this type of secondary structures. However, we find some regions with clearer differences. For example, from residue 200 to 206 there is a considerable discrepancy between the models. In the A chain of the 5ZH8 model there is an α-helix not visible in the others, while in the B chain of our B2X11 model it has not even been possible to model this region. This corroborates that it is a flexible region (Lys204 and Tyr206 are also missing in the Dalal et al., 2019 model), which makes sense, as it is a region highly exposed to the solvent and forms part of the external part of the pocket, so it may require some flexibility be involved in interaction with WTA.

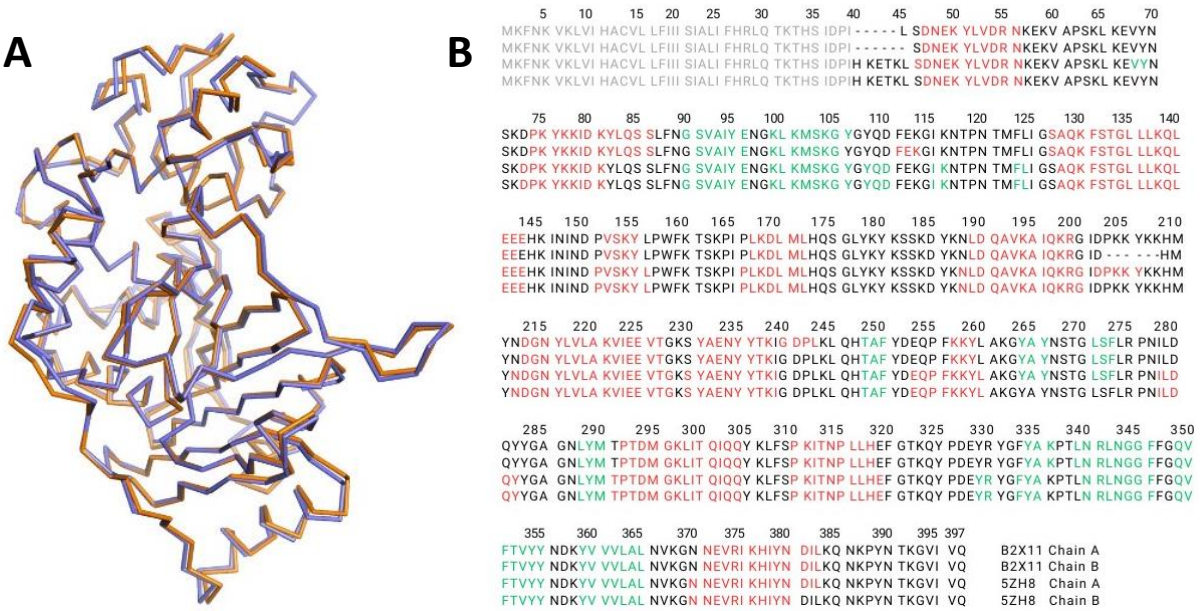


***Figure 9. Comparison of chains structures.*** *A. Superposition of subunits A (blue) and B (orange). Both subunits have a very similar structure, almost identical in the central areas, with some differences in the solvent-exposed areas. It should be noted that at the top right, we can see a non-overlapping area, corresponding to a loop that is missing in subunit B. Comparison between chains A and B of models B2X11 and 5ZH8. The sequences of the four chains under comparison are displayed. Those residues that are not included in the final model are shown in gray. Missing amino acids are denoted by a dash (-). The colours represent the secondary structures: α-helices are depicted in red, while β-sheets are shown in green.*

As mentioned above, the structure of FmtA was solved as a dimer, although Prof. Golemi-Kotra mentioned that FmtA is a monomer in its physiological state. Dalal et al., 2019 reported that at the dimer interface between both chains, there are three weak hydrogen bonds linking the two chains: Ser 85, Lys 368, and Asn370. To address this question, we have studied the interacting surfaces between subunits. We used the PDBePISA (Protein, Interfaces, Surfaces and Assemblies) tool, which, considering a series of criteria that contribute to the stability of molecular complexes, estimates the most stable complex for a given structure. This program uses an algorithm that computes the Complex Formation Significance Score (CSS), a value that ranges between 0 and 1, with a higher value indicating that the interface seen in the crystal structure is more likely to be also found in solution. The CSS obtained was 0.186, which implies that the interface between the A and B chains plays an auxiliary role in complex formation, but is not sufficient to guarantee that both chains form a dimeric complex under physiological conditions. PDBePISA also performs an analysis to define a dimerization interface, as well as the amino acids that form it. In each subunit, there are 24 amino acid residues that form part of the dimerization interface (Figure 10A) and thus potentially contribute to the binding of both chains. These residues make up 6.9% of the total of each subunit. In addition, of these 24 residues, two form hydrogen bonds with the other chain: Lys376 and Tyr334 of chain B, with Tyr266 and Ser268 of chain A, respectively. The hydrogen-bonding residues reported by Dalal et al. (2019) do not coincide with those found in our structure, but they are residues involved in the dimerization surface. One element that should not be overlooked is the central chlorine, located between the two chains. Its peculiar position, right at the dimerization interface, makes it particularly interesting. This chlorine atom within the FmtA structure creates its own interface with each chain, delineating its fundamental role in dimerization. These interfaces have been determined to have a CSS of 0.298 each. This should be taken into account when considering the possibility that FmtA is a dimer in its physiological state. However, the PDBePISA tool cannot account for all three surfaces simultaneously.

In particular, an examination of the structure of FmtA reveals a symmetrical positioning of the chlorine atom between the two chains, surrounded by four residues of each chain and flanked by two symmetrical water molecules. This arrangement underlines the structural importance of both the chlorine atom and its flanking water molecules in dimerization. In Carugo (2014), it is described that when chlorides appear in protein structures, they present a first coordination sphere formed by hydrogen bond donors (N-H and O-H groups) located at about 3.4 Å. Figure 10B shows that within this coordination sphere, the chlorine atom interacts with the two symmetrical water molecules and with the amino groups of the Asn370 of both chains.

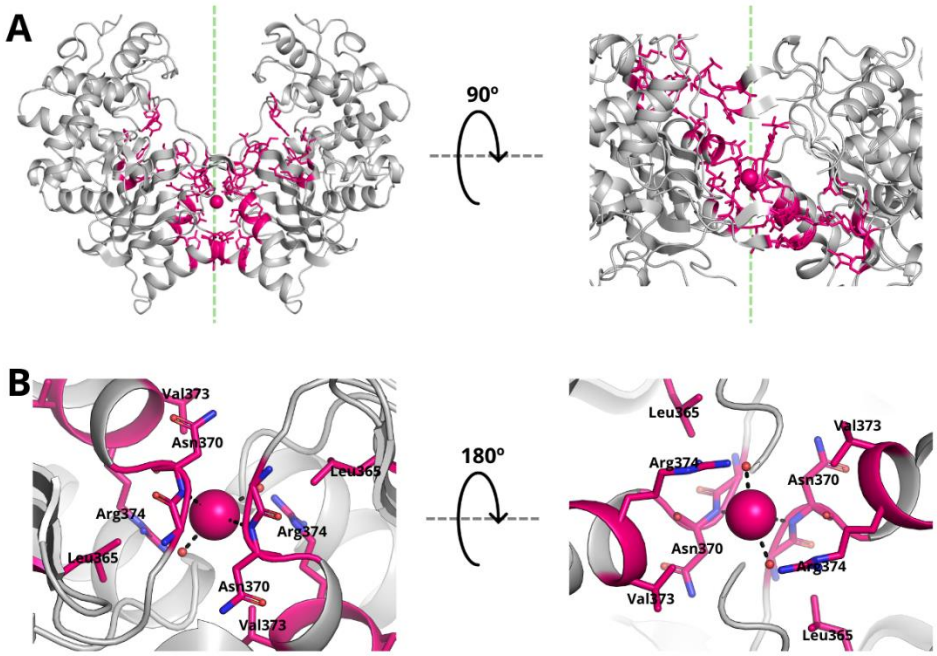


***Figure 10. Comparison of chains structures.*** *A. Dimerisation surface. The amino acids and chain regions that form part of the dimerization surface are shown in pink. Most of them are present in the central region, but there is a part of the interface extending towards the top, where the chains are cross-linked. Most residues that form part of this interaction surface are arranged continuously along different regions of the chains. However, there are also isolated residues that contribute. B. Central chlorine. We observe the central chlorine (in pink), located in the core of FmtA. In pink there are 4 amino acid residues that form an interface with it. In addition, two water molecules are represented as red spheres, and the molecular interactions are represented as dashed black lines.*

FmtA shares several structural features with a large family of proteins, the penicillin binding proteins (PBPs). One of the key aspects of the FmtA structure that it shares with the PBPs is the core structure, which consists of an α/β-domain (consisting of 15 β-strands forming an antiparallel β-sheet flanked by 6 α-helices) and a α-helix region (consisting of 8 α-helices). These domains are folded, with the active site (Figure 11) sandwiched between them.

FmtA retains two of the three typical PBP motifs: SXXK and Y(S)XN. These are of great relevance, as they are part of the active site and are involved in catalysis. According to the kinetic and mutagenesis studies described in Dalal et al., 2019, these motifs provide the hydrogen-bonding network between the active site residues, contributing to their conformation and providing the residues necessary to catalyse the hydrolysis of teichoic acids.

In FmtA, the SXXK motif is located at the N-terminal end of the α3-helix, and includes residues Ser127 and Lys130. Ser127 acts as a nucleophile during catalysis and, as in other PBPs, is surrounded by residues that form a hydrophobic space (suitable for harbouring teichoic acids as substrates). In this motif we also find Lys130, which due to its position at hydrogen bonding distance from Ser127 and Asp213, it is deduced to act as a general base during the acylation reaction by activating Ser127, and to remain stable in its neutral state thanks to Asp213.

Moreover, we have the Y(S)XN motif, where Tyr211 keeps Ser127 positioned in the active site by hydrogen bonding, performing an anchoring function, relevant for the correct positioning of the substrate. In addition, Tyr211 acts as a general base during the deacylation process, as it has hydrogen bonding distance to Ser127 and a water molecule, which it can activate during catalysis. The third residue of this motif is an Asparagine in most PBPs, but in the case of FmtA it is Asp213, which, as mentioned above, acts as a stabiliser of a neutral Lys130. In FmtA, the relationships between Ser127, Lys130 and Asp213 and their functions are similar to the classical catalytic triad of serine proteases (Ser/His/Asp). According to the kinetic and mutagenesis studies of Dalal et al., 2019, Lys130 can assume the role of Tyr211 as a general base during the deacylation reaction; however, the structure was not resolved with any water molecule at the right distance to be activated by Lys130. As no water molecule at a hydrogen bonding distance to Lys130 appears in our model either, we cannot verify this hypothesis.

The active site of FmtA, beyond its catalytic motifs and residues, has additional elements contributing to its structural integrity and stability. These include two structural water molecules, conserved in other PBPs, which are closely involved in promoting the stability of the active site through hydrogen bonding interactions. Despite this stabilising role, they are also expected to exhibit weak nucleophilic activity during catalysis. Also relevant is the function of Tyr282, unique to FmtA among the known PBPs, which forms a vital part of this hydrogen-bonding network, favouring together with Lys130 and Asp213. This arrangement stabilises the protonated state of Lys130 during catalytic processes. A characteristic feature of Tyr282 is that it has a double conformation, and the occupancy of each conformation is very close to 50%, which means that half of the molecules in the crystal will have one conformation and the other half the opposite conformation. This could be relevant to the catalysis process per se or to the entry of the substrate into the active site.

In most PBPs there is a third conserved motif, the KTG box. However, this is not present in FmtA, and instead there is the LNG box, formed by Leu342 Asn343 and Gly344, which contributes to the architecture of the active site of FmtA. The structural function of this motif is to generate a cavity in the active site, which, during catalysis, will house the D-ala of TAs. This is possible thanks to Gly344, which avoids steric clashes with the substrate, and the side chain of Leu342, which is oriented opposite to the active site. In the structural model, this pocket accommodates a water molecule. These residues, which shape the active site, make it a large, loose pocket suitable for interaction with large substrates such as WTAs.

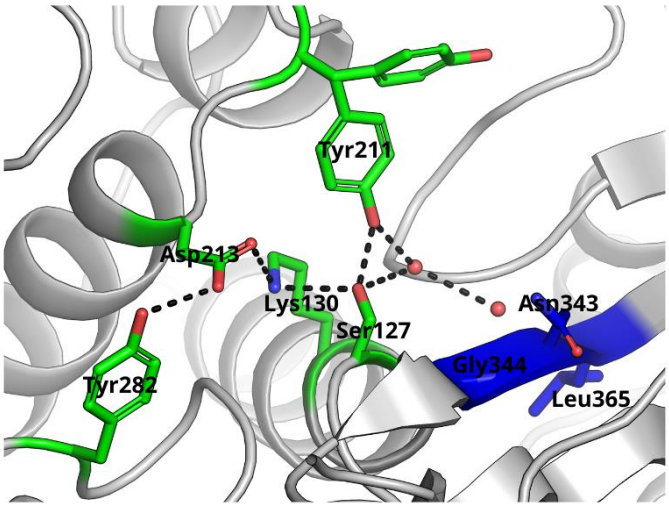


***Figure 11. Active site.*** *The image shows the active site of FmtA. Shown in green the catalytic residues (of SXXK and Y(S)XN motifs), as well as those forming the stable hydrogen-bonding network (both tyrosines). Two water molecules appear as red spheres, and the hydrogen bonds are outlined with black dashed lines. The linearity of the hydrogen bonds stands out, giving rise to a lax and elongated active site. The residues outlined in blue form the LNG box and contribute to the structure of the active site, giving it the slack it requires.*

# 6 CONCLUSIONS

The main objective of the study has been successfully achieved, as we have resumed the collaborative effort with Prof. Dasantila Golemi-Kotra, reproducing the results of Dalal et al., 2019 by obtaining high-quality crystals of the protein FmtA. This achievement has enabled the elucidation of the three-dimensional structure at a higher resolution than previously reported.

In pursuit of this achievement, the following milestones have been reached:

1. The methodologies employed in this study have been fine-tuned for the reproducible and quality expression, purification and crystallisation of the protein FmtA.
2. The new FmtA APO WT model has been solved at a higher level of detail and complexity.
3. The resulting model has enabled a more complete characterisation of FmtA, including the interaction with previously unknown cofactors.

# 7 FUTURE WORK

In this work, we have obtained an improved 3D structure of FmtA WT in its APO form, allowing us to examine in detail some of its elements and structural characteristics.

To further understand FmtA structure and function, additional studies are necessary, such as:

- Crystallizing and solving the structure of FmtA with its ligands or other interacting molecules. Specifically proposed are wall teichoic acids (WTA) as they are physiological ligands, to understand in detail the enzyme-substrate interactions that occur, as well as the role of different residues involved in the catalytic process. It would also be interesting to complex the protein with penicillins and β-lactam antibiotics to understand FmtA resistance mechanisms and be able to target them.
- Mutagenesis studies to investigate the roles of different residues in catalysis, substrate binding, and antibiotic resistance. The S127A mutant crystallized in this project is particularly interesting due to the importance of Ser127 as a residue of the active site and its role in covalent binding to β-lactams. Other residues for which generating mutants may be interesting include Lys130, Asp213, Tyr211. These mutants are of great interest for structural and kinetic studies.

All of this provides us with a knowledge base to exploit the potential of FmtA as a therapeutic target and to develop possible drugs to combat Staphylococcus aureus. Obtaining 3D structures provides us with a model for conducting various in silico assays. This is highly relevant for structure-based drug design (SBDD), as it employs computational methodologies such as:

- Docking to characterize the binding affinity of the protein with drugs. It is mainly used to search for candidates in databases of active compounds, based on electrostatic and steric interactions with the binding site.
- Molecular dynamics simulations to study protein-drug bonds and interactions and evaluate the stability of the complex.
- Molecular mechanics to determine the structural and conformational variations that the protein undergoes after binding to the drug.

These techniques allow the search for new pharmacological compounds that have potential interactions with the therapeutic target, turning 3D structures into an efficient technology to accelerate the drug discovery process (Martin et al., 2024).

# 8 REFERENCES


AGIRRE, J., MIHAELA , A., BAGDONAS, H., BALLARD, C., ARNAUD , B., BEILSTEN-EDMANDS, J., BORGES, R. J., BROWN, D. G., JOSÉ JAVIER BURGOS-MÁRMOL, BERRISFORD, J. M., BOND, P. S., CABALLERO, I., CATAPANO, L., CHOJNOWSKI, G., COOK, A. G., COWTAN, K., CROLL, T. I., J. DEBRECZENI, DEVENISH, N. E., & DODSON, E. J. (2023). The *CCP*4 suite: integrative software for macromolecular crystallography. *Acta Crystallographica Section D: Structural Biology*, *79*(6), 449–461. https://doi.org/10.1107/s2059798323003595

BALABAN, N. Q., HELAINE, S., LEWIS, K., ACKERMANN, M., ALDRIDGE, B., ANDERSSON, D. I., BRYNILDSEN, M. P., BUMANN, D., CAMILLI, A., COLLINS, J. J., DEHIO, C., FORTUNE, S., GHIGO, J.-M., HARDT, W.-D., HARMS, A., HEINEMANN, M., HUNG, D. T., JENAL, U., LEVIN, B. R., & MICHIELS, J. (2019). Definitions and guidelines for research on antibiotic persistence. *Nature Reviews Microbiology*, *17*(7), 441–448. https://doi.org/10.1038/s41579-019-0196-3

BROWN, S., SANTA MARIA, J. P., & WALKER, S. (2013). Wall teichoic acids of gram-positive bacteria. *Annual Review of Microbiology*, *67*(1), 313–336. https://doi.org/10.1146/annurev-micro-092412-155620

CHAIT, R., CRANEY, A., & KISHONY, R. (2007). Antibiotic interactions that select against resistance. *Nature*, *446*(7136), 668–671. https://doi.org/10.1038/nature05685

CHALMERS, S. J., & WYLAM, M. E. (2020). Methicillin-Resistant Staphylococcus aureus Infection and Treatment Options. *Methods in Molecular Biology (Clifton, N.J.)*, *2069*, 229–251. https://doi.org/10.1007/978-1-4939-9849-4_16

CHAMBERS, H. F. (1997). Methicillin resistance in staphylococci: molecular and biochemical basis and clinical implications. *Clinical Microbiology Reviews*, *10*(4), 781–791. https://doi.org/10.1128/cmr.10.4.781-791.1997

CHAMBERS, H. F., & DELEO, F. R. (2009). Waves of resistance: Staphylococcus aureus in the antibiotic era. *Nature Reviews Microbiology*, *7*(9), 629–641. https://doi.org/10.1038/nrmicro2200

CHEUNG, G. Y. C., BAE, J. S., & OTTO, M. (2021). Pathogenicity and virulence of Staphylococcus aureus. *Virulence*, *12*(1), 547–569. https://doi.org/10.1080/21505594.2021.1878688

COLLINS, L. V., KRISTIAN, S. A., WEIDENMAIER, C., FAIGLE, M., VAN KESSEL, K. P. M., VAN STRIJP, J. A. G., GÖTZ, F., NEUMEISTER, B., & PESCHEL, A. (2002). Staphylococcus aureus strains lacking D-alanine modifications of teichoic acids are highly susceptible to human neutrophil killing and are virulence attenuated in mice. *The Journal of Infectious Diseases*, *186*(2), 214–219. https://doi.org/10.1086/341454

DALAL, V., DHANKHAR, P., SINGH, V., SINGH, V., RAKHAMINOV, G., GOLEMI-KOTRA, D., & KUMAR, P. (2021). Structure-Based Identification of Potential Drugs Against FmtA of Staphylococcus aureus: Virtual Screening, Molecular Dynamics, MM-GBSA, and QM/MM. *The Protein Journal*, *40*(2), 148–165. https://doi.org/10.1007/s10930-020-09953-6

DALAL, V., KUMAR, P., RAKHAMINOV, G., QAMAR, A., FAN, X., HUNTER, H., TOMAR, S., GOLEMI-KOTRA, D., & KUMAR, P. (2019). Repurposing an Ancient Protein Core Structure: Structural Studies on FmtA, a Novel Esterase of Staphylococcus aureus. *Journal of Molecular Biology*, *431*(17), 3107–3123. https://doi.org/10.1016/j.jmb.2019.06.019

DE OLIVEIRA, D. M. P., FORDE, B. M., KIDD, T. J., HARRIS, P. N. A., SCHEMBRI, M. A., BEATSON, S. A., PATERSON, D. L., & WALKER, M. J. (2020). Antimicrobial Resistance in ESKAPE Pathogens. *Clinical Microbiology Reviews*, *33*(3). https://doi.org/10.1128/cmr.00181-19

DESSAU, M. A., & MODIS, Y. (2011). Protein crystallization for X-ray crystallography. *Journal of Visualized Experiments*, *47*(47). https://doi.org/10.3791/2285

EMSLEY, P., LOHKAMP, B., SCOTT, W. G., & COWTAN, K. (2010). Features and development ofCoot. *Acta Crystallographica Section D Biological Crystallography*, *66*(4), 486–501.

https://doi.org/10.1107/s0907444910007493
ENRIGHT, M. C., ROBINSON, D. A., RANDLE, G., FEIL, E. J., GRUNDMANN, H., & SPRATT, B. G. (2002). The evolutionary history of methicillin-resistant Staphylococcus aureus (MRSA). *Proceedings of the National Academy of Sciences*, *99*(11), 7687–7692. https://doi.org/10.1073/pnas.122108599
FAN, X., LIU, Y., SMITH, D., KONERMANN, L., SIU, K. W. M., & GOLEMI-KOTRA, D. (2007). Diversity of Penicillin-binding Proteins. Resistance factor FmtA of Staphylococcus Aureus. *Journal of Biological Chemistry*, *282*(48), 35143–35152. https://doi.org/10.1074/jbc.M706296200
GASTEIGER, E., HOOGLAND, C., GATTIKER, A., DUVAUD, S., WILKINS, M. R., APPEL, R. D., & BAIROCH, A. (2005). Protein Identification and Analysis Tools on the ExPASy Server. *The Proteomics Protocols Handbook*, 571–607. https://doi.org/10.1385/1-59259-890-0:571
GORWITZ, RACHEL J., KRUSZON-MORAN, D., MCALLISTER, SIGRID K., MCQUILLAN, G., MCDOUGAL, LINDA K., FOSHEIM, GREGORY E., JENSEN, BETTE J., KILLGORE, G., TENOVER, FRED C., & KUEHNERT, MATTHEW J. (2008). Changes in the Prevalence of Nasal Colonization withStaphylococcus aureusin the United States, 2001–2004. *The Journal of Infectious Diseases*, *197*(9), 1226–1234. https://doi.org/10.1086/533494
GRUNDMANN, H., AIRES-DE-SOUSA, M., BOYCE, J., & TIEMERSMA, E. (2006). Emergence and resurgence of meticillin-resistant Staphylococcus aureus as a public-health threat. *The Lancet*, *368*(9538), 874–885. https://doi.org/10.1016/s0140-6736(06)68853-3
GUO, Y., SONG, G., SUN, M., WANG, J., & WANG, Y. (2020). Prevalence and Therapies of Antibiotic-Resistance in Staphylococcus aureus. *Frontiers in Cellular and Infection Microbiology*, *10*(107). https://doi.org/10.3389/fcimb.2020.00107
HASHMI, H. B., FAROOQ, M. A., KHAN, M. H., ALSHAMMARI, A., ALJASHAM, A. T., RASHID, S. A., KHAN, N. R., HASHMI, I. B., BADAR, M., & MUBARAK, M. S. (2023). Collaterally Sensitive β-Lactam Drugs as an Effective Therapy against the Pre-Existing Methicillin Resistant Staphylococcus aureus (MRSA) Biofilms. *Pharmaceuticals*, *16*(5), 687–687. https://doi.org/10.3390/ph16050687
KLUYTMANS, J., VAN BELKUM, A., & VERBRUGH, H. (1997). Nasal carriage of Staphylococcus aureus: epidemiology, underlying mechanisms, and associated risks. *Clinical Microbiology Reviews*, *10*(3), 505–520. https://doi.org/10.1128/cmr.10.3.505
KOMATSUZAWA, H., OHTA, K., LABISCHINSKI, H., SUGAI, M., & SUGINAKA, H. (1999). Characterization of fmtA, a Gene That Modulates the Expression of Methicillin Resistance in Staphylococcus aureus. *Antimicrobial Agents and Chemotherapy*, *43*(9), 2121–2125. https://doi.org/10.1128/aac.43.9.2121
KOMATSUZAWA, H., SUGAI, M., OHTA, K., FUJIWARA, T., NAKASHIMA, S., SUZUKI, J., LEE, C. Y., & SUGINAKA, H. (1997). Cloning and characterization of the fmt gene which affects the methicillin resistance level and autolysis in the presence of triton X-100 in methicillin-resistant Staphylococcus aureus. *Antimicrobial Agents and Chemotherapy*, *41*(11), 2355–2361. https://doi.org/10.1128/aac.41.11.2355
KRISSINEL, E., & HENRICK, K. (2007). Inference of macromolecular assemblies from crystalline state. *Journal of Molecular Biology*, *372*(3), 774–797. https://doi.org/10.1016/j.jmb.2007.05.022
LÁZÁR, V., SNITSER, O., BARKAN, D., & KISHONY, R. (2022). Antibiotic combinations reduce Staphylococcus aureus clearance. *Nature*, *610*(540–546), 1–7. https://doi.org/10.1038/s41586-022-05260-5
LEE, A. S., DE LENCASTRE, H., GARAU, J., KLUYTMANS, J., MALHOTRA-KUMAR, S., PESCHEL, A., & HARBARTH, S. (2018). Methicillin-resistant Staphylococcus aureus. *Nature Reviews. Disease Primers*, *4*(18033), 18033. https://doi.org/10.1038/nrdp.2018.33
LOWY, F. D. (1998). Staphylococcus aureus infections. *The New England Journal of Medicine*, *339*(8), 520–532. HTTPS://DOI.ORG/10.1056/NEJM199808203390806
MARTIN, R. L., HEIFETZ, A., BODKIN, M. J., & TOWNSEND-NICHOLSON, A. (2024). High-

Throughput Structure-Based Drug Design (HT-SBDD) Using Drug Docking, Fragment Molecular Orbital Calculations, and Molecular Dynamic Techniques. *Methods in Molecular Biology (Clifton, N.J.)*, *2716*, 293–306. https://doi.org/10.1007/978-1-0716-3449-3_13

MCALEESE, F., WU, S. W., SIERADZKI, K., DUNMAN, P., MURPHY, E., PROJAN, S., & TOMASZ, A. (2006). Overexpression of Genes of the Cell Wall Stimulon in Clinical Isolates of Staphylococcus aureus Exhibiting Vancomycin Intermediate S. aureus Type Resistance to Vancomycin. *Journal of Bacteriology*, *188*(3), 1120–1133. https://doi.org/10.1128/jb.188.3.1120-1133.2006

MCCALLUM, N., SPEHAR, G., BISCHOFF, M., & BERGER-BÄCHI, B. (2006). Strain dependence of the cell wall-damage induced stimulon in Staphylococcus aureus. *Biochimica et Biophysica Acta (BBA) - General Subjects*, *1760*(10), 1475–1481. https://doi.org/10.1016/j.bbagen.2006.06.008

MLYNARCZYK-BONIKOWSKA, B., KOWALEWSKI, C., KROLAK-ULINSKA, A., & MARUSZA, W. (2022). Molecular Mechanisms of Drug Resistance in Staphylococcus aureus. *International Journal of Molecular Sciences*, *23*(15), 8088. https://doi.org/10.3390/ijms23158088

NEUHAUS, F. C., & BADDILEY, J. (2003). A continuum of anionic charge: Structures and functions of D-alanyl-teichoic acids in gram-positive bacteria. *Microbiology and Molecular Biology Reviews*, *67*(4), 686–723. https://doi.org/10.1128/mmbr.67.4.686-723.2003

OLIVIERO CARUGO. (2014). Buried chloride stereochemistry in the Protein Data Bank. *BMC Structural Biology*, *14*(1). https://doi.org/10.1186/s12900-014-0019-8

RAHMAN, M. M., HUNTER, H. N., PROVA, S., VERMA, V., QAMAR, A., & GOLEMI-KOTRA, D. (2016). The Staphylococcus aureus methicillin resistance factor Fmta is a d-Amino esterase that acts on teichoic acids. *MBio*, *7*(1). https://doi.org/10.1128/mbio.02070-15

RAJAGOPAL, A., DEMBIA, C. L., DEMERS, M. S., DELP, D. D., HICKS, J. L., & DELP, S. L. (2016). Full-Body Musculoskeletal Model for Muscle-Driven Simulation of Human Gait. *IEEE Transactions on Biomedical Engineering*, *63*(10), 2068–2079. https://doi.org/10.1109/tbme.2016.2586891

READ, R. J., ADAMS, P. D., ARENDALL, W. B., BRUNGER, A. T., EMSLEY, P., JOOSTEN, R. P., KLEYWEGT, G. J., KRISSINEL, E., LÜTTEKE, T., ZBYSZEK OTWINOWSKI, ANASTASSIS PERRAKIS, RICHARDSON, J. S., SHEFFLER, W., SMITH, J. L., TICKLE, I. J., GERT VRIEND, & ZWART, P. H. (2011). A New Generation of Crystallographic Validation Tools for the Protein Data Bank. *Structure*, *19*(10), 1395–1412. https://doi.org/10.1016/j.str.2011.08.006

SAMBROOK, J., & RUSSEL, D. W. (2001). *Molecular cloning a laboratory manual* (Fourth Edition). Cold Spring Harbor Laboratory Press.

SINGH, V., POONAM DHANKHAR, DALAL, V., TOMAR, S., DASANTILA GOLEMI-KOTRA, & KUMAR, P. (2022). Drug-Repurposing Approach To Combat *Staphylococcus aureus*: Biomolecular and Binding Interaction Study. *ACS Omega*, *7*(43), 38448–38458. https://doi.org/10.1021/acsomega.2c03671

TASNEEM, U., MAJID, M., MEHMOOD, K., REDAINA, UR REHMAN, F., ANDLEEB, S., & JAMAL, M. (2022). Co-occurrence of antibiotic resistance and virulence Genes in Methicillin Resistant Staphylococcus aureus (MRSA) Isolates from Pakistan. *African Health Sciences*, *22*(1), 486–495. https://doi.org/10.4314/ahs.v22i1.57

TURNER, N. A., SHARMA-KUINKEL, B. K., MASKARINEC, S. A., EICHENBERGER, E. M., SHAH, P. P., CARUGATI, M., HOLLAND, T. L., & FOWLER, V. G. (2019). Methicillin-resistant Staphylococcus aureus: an overview of basic and clinical research. *Nature Reviews. Microbiology*, *17*(4), 203–218. https://doi.org/10.1038/s41579-018-0147-4

UTAIDA, S., DUNMAN, P. M., MACAPAGAL, D., MURPHY, E., SINGH, S. J., JAYASWAL , R. K., & WILKINSON, B. J. (2003). Genome-wide transcriptional profiling of the response of Staphylococcus aureus to cell-wall-active antibiotics reveals a cell-wall-stress stimulon.

*Microbiology*, *149*(10), 2719–2732. https://doi.org/10.1099/mic.0.26426-0

VAGIN, A. A., STEINER, R. A., LEBEDEV, A. A., POTTERTON, L., MCNICHOLAS, S., LONG, F., & MURSHUDOV, G. N. (2004). REFMAC5 dictionary: organization of prior chemical knowledge and guidelines for its use. *Acta Crystallographica Section D Biological Crystallography*, *60*(12), 2184–2195. https://doi.org/10.1107/s0907444904023510

VONRHEIN, C., FLENSBURG, C., KELLER, P., SHARFF, A., SMART, O., PACIOREK, W., WOMACK, T., & BRICOGNE, G. (2011). Data processing and analysis with theautoPROCtoolbox. *Acta Crystallographica Section D Biological Crystallography*, *67*(4), 293–302. https://doi.org/10.1107/s0907444911007773

WERTHEIM, H. F., MELLES, D. C., VOS, M. C., VAN LEEUWEN, W., VAN BELKUM, A., VERBRUGH, H. A., & NOUWEN, J. L. (2005). The role of nasal carriage in Staphylococcus aureus infections. *The Lancet Infectious Diseases*, *5*(12), 751–762. https://doi.org/10.1016/s1473-3099(05)70295-4

WLODAWER, A., MINOR, W., DAUTER, Z., & JASKOLSKI, M. (2007). Protein crystallography for non-crystallographers, or how to get the best (but not more) from published macromolecular structures. *FEBS Journal*, *275*(1), 1–21. https://doi.org/10.1111/j.1742-4658.2007.06178.x